Nucleation and growth of helium bubbles in nickel studied by positron-annihilation spectroscopy

G. Amarendra, B. Viswanathan, A. Bharathi, and K. P. Gopinathan
Materials Science Division, Indira Gandhi Centre for Atomic Research, Kalpakkam 603 102, Tamil Nadu, India
(Received 22 July 1991; revised manuscript received 24 October 1991)

Positron-annihilation spectroscopy (PAS) has been used for the study of the behavior of helium in nickel. Helium has been homogeneously implanted in pure nickel by α-particle irradiation with use of a cyclotron. Post-implantation positron-lifetime and Doppler-broadened line-shape measurements have been carried out as a function of the isochronal annealing temperature on the samples containing 100 and 400 at. ppm of helium. The marked changes in the annihilation parameters, observed around 750 K in the helium-implanted Ni (100 at. ppm He), absent in the recovery of helium-free irradiated Ni, have been identified with bubble nucleation. In order to understand the effect of helium decoration of vacancies on the positron lifetime, *ab initio* theoretical calculations have been carried out as a function of the vacancy-cluster size and helium-to-vacancy ratio in the clusters. The computed positron lifetimes have been used to interpret the experimental PAS results in the bubble-nucleation stage. In the post-nucleation growth stage above 750 K, the bubble parameters, viz., bubble size and bubble concentration, have been extracted from an analysis of PAS data. An analysis of bubble growth in Ni indicates the existence of overpressurized bubbles and the implication of this result on bubble-growth mechanisms is discussed. The helium-dose dependence of the bubble parameters is also evaluated from these experimental PAS results.

I. INTRODUCTION

The study of helium in metals is of both fundamental and technological interest.[1-3] Being a closed-shell atom, helium interacts repulsively with metal atoms and hence has a very low solubility in metals. It is effectively trapped at open-volume defects such as vacancies, dislocations, and grain boundaries. Preferential clustering of helium around these defects lead to the formation of helium bubbles, which results in the degradation of the mechanical properties of materials used in fission and fusion reactors.[3] Detailed study of the properties of helium bubbles in nickel is of particular importance, since nickel is a model metal for some of the steel alloys used in irradiation environments.

Various experimental techniques[4,5] have been used in studying helium behavior in metals. Detailed transmission-electron-microscopy (TEM) studies[6] on proton and α-particle irradiated Ni have yielded information about the post-irradiation microstructure and growth of large bubbles. Thermal helium-release experiments[7,8] have provided information about helium-migration mechanisms in Ni. The thermal stability of different helium-vacancy complexes in Ni has been investigated by thermal helium-desorption-spectroscopy (THDS) studies.[8,9] Theoretical estimates of binding energies of various helium-vacancy complexes in Ni have also been reported.[10,11] A recent systematic TEM study in nickel[12] has revealed the existence of different coarsening mechanisms for the growth of bubbles in the bulk and near the surface. Very recently, small-angle neutron-scattering (SANS) combined with TEM measurements[13] have been reported on helium-implanted nickel. These studies reveal the existence of overpressurized bubbles in Ni, even at an annealing temperature above $0.7T_m$.

Positron-annihilation spectroscopy (PAS) is a powerful technique for the study of small submicroscopic vacancy-type clusters. This technique has been widely used for the size determination of microvoids and for the study of impurity-void interactions in metals and alloys.[14,15] The effect of helium decoration of voids on positron-annihilation characteristics in fcc metals has been studied with *ab initio* theoretical calculations by Jena and Rao.[16] More recently, Jensen and Nieminen[17,18] have reported detailed molecular-dynamics and positron-lifetime calculations in Al to obtain a relation between the helium-atom density and lifetime for the bubbles above a critical size. In the small-cluster regime (radius < 5 Å), the positron lifetime is found to be sensitive to the size as well as the helium-to-vacancy ratio in the cluster.[18] Thus the defect specificity of PAS, combined with its sensitivity to helium decoration, could be effectively used for a qualitative and quantitative understanding of properties of helium bubbles over a wide size range.

PAS studies of helium-implanted aluminum[19-21] and copper[22,23] have led to a detailed understanding of nucleation and growth of bubbles. In a PAS study[24] on Ni, homogeneously implanted with helium, various annealing stages of helium were identified and compared with those of stainless steel 316. In another PAS study on Ni, irradiated with monoenergetic 30-MeV α particles, post-irradiation Doppler-broadening, and lifetime measurements[25] did not reveal clear stages corresponding to helium bubbles. A third PAS study on homogeneously helium-implanted nickel[26] provided a qualitative understanding of helium decoration of vacancies and also the temperature dependence of positron trapping in bubbles. However, a comprehensive and quantitative knowledge of the nucleation and growth of helium bubbles in nickel has been still lacking. In the present paper, combined

theoretical and experimental investigations toward this objective are reported. The present work addresses the following: (i) *ab initio* theoretical calculations of positron lifetime and an understanding of the effect of helium decoration of vacancy clusters, (ii) clear identification of the nucleation and growth stages of helium bubbles by detailed PAS measurements on helium-implanted Ni and comparison with helium-free irradiated Ni samples, (iii) analysis of PAS data and the extraction of bubble parameters such as bubble radius, bubble concentration, and helium pressure in the growth stage, and (iv) study of the effect of helium dose on bubble parameters in Ni. A part of the results has been reported earlier.[27]

The paper is organized as follows: In Sec. II the computational results of positron-annihilation characteristics in various helium-vacancy clusters and multiple-helium–single-vacancy complexes are presented. The experimental details are furnished in Sec. III. The PAS results on α-particle-irradiated Ni samples containing 100 at. ppm He are discussed in Sec. IV. The scheme employed for the analysis of bubble coarsening is described and the deduced bubble parameters for Ni (100 at. ppm He) are presented and discussed in Sec. V. PAS results corresponding to α-particle-irradiated Ni containing 400 at. ppm He are presented in Sec. VI. The dependence of bubble parameters on helium dose is discussed in Sec. VII. Section VIII gives a summary and conclusion.

II. COMPUTATIONAL RESULTS: POSITRON-LIFETIME CHARACTERISTICS

In this section the computational results of the effect of helium decoration of vacancy clusters on positron-lifetime characteristics are presented. For small helium-vacancy clusters, positron samples the free volume of the defect, wherein the positron lifetime is sensitive to the size as well as the helium-to-vacancy ratio in the cluster.[18] Accordingly, the calculations have been carried out on two different types of helium-vacancy clusters, viz., (i) He-V clusters having the same helium-to-vacancy ratio N_{He}/N_V, but varying in size, to study the variation of lifetime with cluster size and (ii) He-V complexes with fixed size and varying N_{He}/N_V ratio to study the influence of the latter on lifetime. A brief outline of the method[28,29] is given below.

First, the positron potential is written as a sum of Hartree electrostatic potential due to ions and electrons and the positron-electron correlation potential. The latter is obtained from many-body calculations,[30] within the local-density approximation. The electrostatic potential and electron density of the solid are approximated by a superposition of atomic potentials and densities. The atomic potentials and densities are obtained from the self-consistent Hartree-Fock calculations.[31] The total positron potential given by the above prescription has been computed for various helium-vacancy complexes of appropriate structure, in a fcc Ni matrix containing 1372 atoms. The potential has been evaluated on a three-dimensional grid with a grid size of ~ 0.50 a.u. The Schrödinger equation has been solved in real space with this positron potential, using the finite-difference scheme to obtain the positron wave function. The total annihilation rate is evaluated as a sum of valence- and core-annihilation rates.[28,29] For the Ni atom, the $4s^2$ electrons are treated as valence electrons, while the rest are treated as core electrons. For the helium atom, the $1s$ electrons are treated as core electrons. The annihilation rate due to valence electrons is evaluated using the Brandt-Reinheimer interpolation formula.[32] The annihilation rate due to core electrons is calculated in the independent-particle approximation, with a constant enhancement factor of 1.5 for Ni atoms and 1.0 for helium atoms.[28]

A. Helium-vacancy clusters

Figure 1(a) shows the isometric plot of the computed positron-density distribution (PDD) in a monovacancy in a Ni lattice, and Fig. 1(b) shows the corresponding contour plot. As is evident from the PDD shown in Fig. 1(a), the positron is localized at the center of the monova-

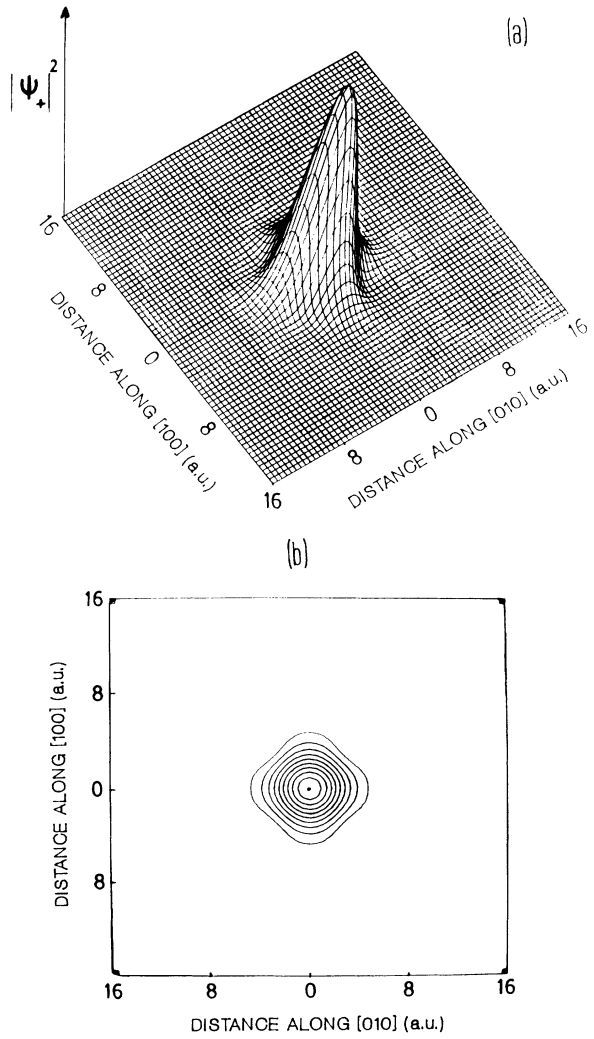

FIG. 1. Computed positron-density distribution in a monovacancy in Ni shown as (a) isometric plot and (b) contour plot. The spacing in the contour plot is $\frac{1}{11}$ the maximum value.

cancy. For the case of a monovacancy decorated with a helium atom (HeV), the isometric and contour plots of the PDD are shown in Figs. 2(a) and 2(b), respectively. Comparison of Figs. 1(a) and 2(a) shows that a "central hole" appears in the PDD of the substitutional helium atom. Because of the presence of helium core at the center of the vacancy in the case of HeV, the positron is pushed away from the center, resulting in the exclusion of the positron from the center of the complex.

The variation of the normalized core-annihilation rate $\lambda_c/(\lambda_c+\lambda_v)$ as a function of cluster size (number of vacancies, N_V, in the cluster) is shown in Fig. 3(a) for pure vacancy and He-V clusters. The normalized core-annihilation rate is found to be larger for He-V clusters than for pure vacancy clusters for all cluster sizes. This increase is brought about by the enhanced core-electron density due to helium decoration of vacancy clusters. As is evident from Fig. 3, the normalized core-annihilation rate for pure vacancy clusters almost vanishes beyond 43 atom-cluster size. In the case of He-V clusters, the normalized core-annihilation rate decreases and remains nearly constant for clusters larger than 43 atoms in size. The variation of the positron lifetime τ, computed from the valence- and core-annihilation rates, as a function of cluster size is shown in Fig. 3(b). In the case of a pure vacancy, the lifetime is 174 ps, and as the cluster size is increased, τ increases and tends to saturate at the void lifetime of 500 ps. The lifetime values obtained as a function of vacancy-cluster size are in agreement with those reported earlier.[28] For HeV the lifetime is $\sim$114 ps, which is markedly lower than that of a pure vacancy. As the He-V cluster size is increased, τ increases initially before tending to level off. The size dependence of τ becomes

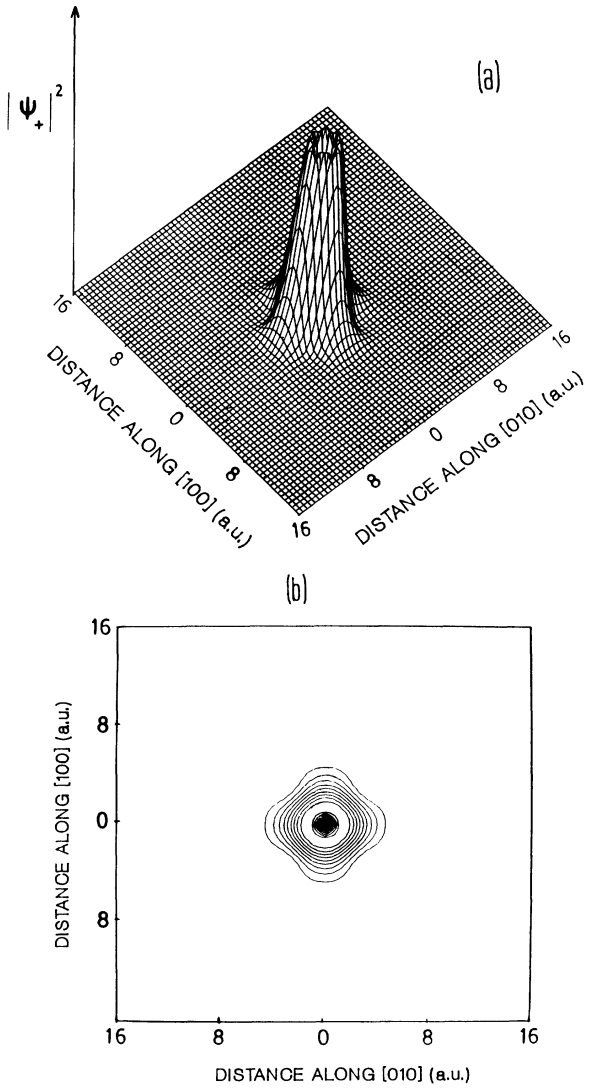

FIG. 2. Computed positron-density distribution in helium-vacancy complex HeV shown as (a) isometric plot and (b) contour plot. The spacing in the contour plot is $\frac{1}{11}$ the maximum value.

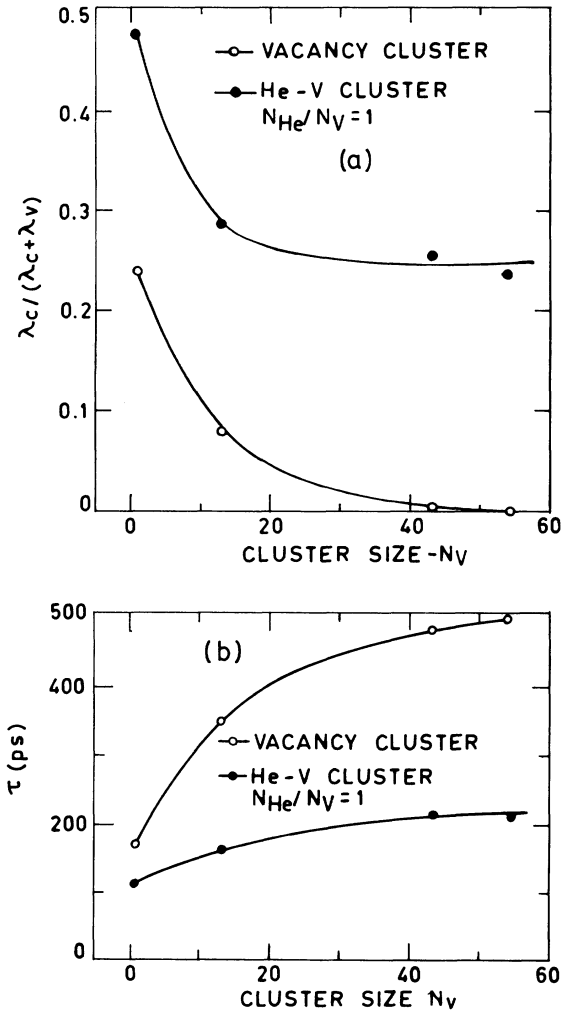

FIG. 3. (a) Variation of the normalized core-annihilation rate $\lambda_c/(\lambda_c+\lambda_v)$ as a function of cluster size (number of vacancies) for pure vacancy clusters (open circles) and for He-V clusters (solid circles) in Ni. (b) Variation of computed positron lifetime τ as a function of cluster size for pure vacancy clusters (open circles) and He-V clusters (solid circles) in Ni. All of the He-V clusters have the same helium-to-vacancy ratio (N_{He}/N_V) of unity.

TABLE I. Computed positron-annihilation characteristics of vacancy clusters and helium-vacancy clusters in Ni. λ_c and λ_v are the core- and valency-annihilation rates. τ is the resultant positron lifetime, and E_B is the positron binding energy in the cluster.

Cluster	λ_c (ns^{-1})	λ_v (ns^{-1})	τ (ps)	E_B (eV)
$1V$	1.3912	4.3685	173.6	−2.60
$13V$	0.2310	2.6137	351.5	−3.34
$43V$	0.00916	2.0664	481.8	−4.36
$54V$	0.00125	2.0222	494.2	−4.39
$1V$+1He	4.1743	4.6236	113.6	−2.32
$13V$+13He	1.7223	4.2756	166.7	−4.21
$43V$+43He	1.1966	3.4691	214.3	−4.66
$54V$+54He	1.1204	3.6084	211.3	−4.72

insignificant for clusters larger than 43 atoms in size. Table I summarizes the results of annihilation characteristics of pure vacancy clusters and He-V clusters.

B. Multiple-helium — vacancy complexes

The results discussed in the previous section pertain to He-V clusters of various sizes having a fixed ratio of N_{He}/N_V equal to unity. It will be of interest to obtain the response of a positron to multiple helium decoration of a single vacancy, i.e., as the ratio of N_{He}/N_V is varied without changing the number of vacancies. The stability of helium-vacancy complexes such as HeV, He$_4V$, and He$_6V$ is known from the results[9–11] of computed binding energies and THDS experiments. The positron-lifetime characteristics for the above complexes are discussed in this section. Since the behavior of the positron lifetime with regard to a pure vacancy ($N_{He}/N_V=0$) and substitutional helium atom ($N_{He}/N_V=1$) is already obtained (Sec. II A), the annihilation characteristics have been computed for a single vacancy decorated with four helium atoms (He$_4V$, $N_{He}/N_V=4$) and a single vacancy decorated with six helium atoms (He$_6V$, $N_{He}/N_V=6$).

The positron lifetime is sensitive to the relative positions of the decorating impurity atoms around the vacancy[33] and hence to the configuration of the defect complex. In view of this, lattice statics calculations[34] have been performed for He$_4V$ and He$_6V$ complexes to obtain the relaxed positions of the decorating helium atoms around a central vacancy. In the present lattice statics calculations, the He$_n V$ complex is located at the center of the computational Ni cell. The form of the Ni-Ni pair potential is taken as suggested by Baskes and Melius,[35] Ni-He pair potential of the Born-Mayor form,[34] and He-He pair potential taken as Lennard-Jones type.[34] By minimizing the elastic forces around the defect using the Newton-Raphson method,[34] the energetically stable configuration of the complex is obtained. The computational details of the method employed are explained elsewhere.[36] The relaxed interstitial helium positions, in units of a half lattice constant of Ni, for He$_4V$ are obtained as (0.7482,0,0), (−0.7482,0,0), (0,0.7482,0), and (0,−0.7482,0). For the He$_6V$ complex, the helium atoms are located at (0.7874,0,0), (−0.7874,0,0), (0,0.7874,0), (0,−0.7874,0), (0,0,0.7874), and (0,0,−0.7874). In these complexes the vacancy is located at the origin (0,0,0).

Figures 4(a) and 4(b) show the isometric and contour plots of the PDD for a He$_4V$ complex. It is clear from the figure that the positron wave function peaks at the site of the central vacancy, exhibiting shallow minima at helium-core positions. The computed annihilation characteristics are shown in Table II for a monovacancy ($N_{He}/N_V=0$), HeV ($N_{He}/N_V=1$), He$_4V$ complex ($N_{He}/N_V=4$), and He$_6V$ complex ($N_{He}/N_V=6$). Figure 5(a) shows the variation of the normalized core-annihilation rate as a function of the N_{He}/N_V ratio. It is noticeable from Fig. 5(a) that the normalized core-annihilation rates for He$_4V$ and He$_6V$ are lower than that of HeV. This is explained as follows: The helium atom is located right at the center of a vacancy for the HeV complex. On the other hand, the helium atoms are situated around the vacancy at off-center interstitial positions for He$_4V$ and He$_6V$ complexes. The larger overlap of the

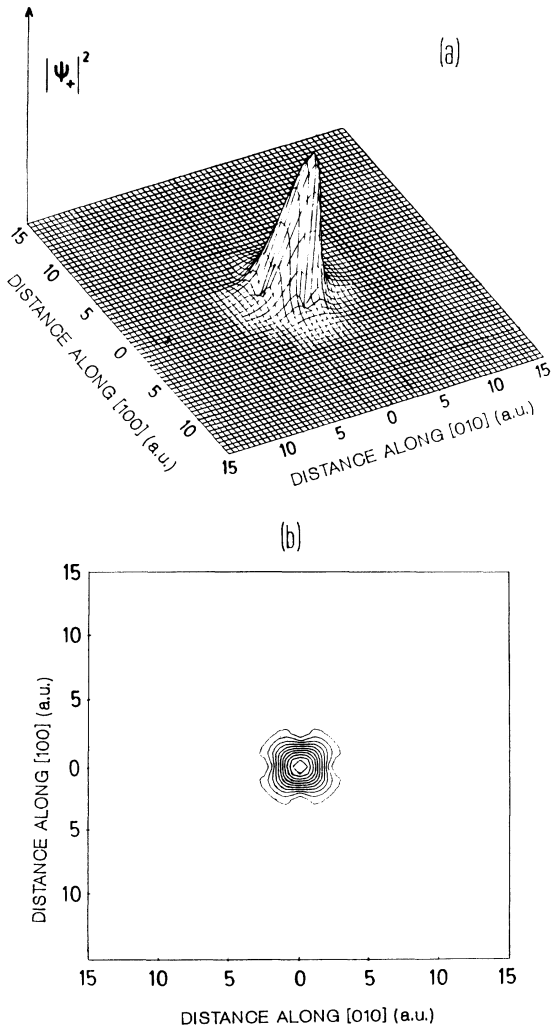

FIG. 4. Computed positron-density distribution in a He$_4V$ complex shown as (a) isometric plot and (b) contour plot. The spacing in the contour plot is $\frac{1}{11}$ the maximum value.

TABLE II. Computed positron-annihilation characteristics of a vacancy and multiple-helium–vacancy complexes in Ni. Here E_B is the positron binding energy to the defect, λ_c and λ_v are the core- and valence-annihilation rates, and τ is positron lifetime in the defect.

Defect	E_B (eV)	λ_c (ns^{-1})	λ_v (ns^{-1})	τ (ps)
$1V$ ($N_{He}/N_V=0$)	−2.60	1.3912	4.3685	173.6
$1V+1$He ($N_{He}/N_V=1$)	−2.32	4.1743	4.6236	113.6
$1V+4$He ($N_{He}/N_V=4$)	−2.21	2.7407	4.4917	138.3
$1V+6$He ($N_{He}/N_V=6$)	−2.09	3.4060	4.5395	125.8

positron density with the core-electron density for the case of HeV, as opposed to that in He_4V and He_6V complexes, results in a larger core-annihilation rate in the former. Owing to the presence of an additional two helium atoms in the He_6V complex, the normalized core-annihilation rate is higher for the He_6V than for the He_4V complex. The corresponding variation of the computed positron lifetime τ as a function of the N_{He}/N_V ratio is shown in Fig. 5(b). The above results clearly demonstrate the influence of the details of the configuration of the multiple-helium–vacancy complexes on the lifetime characteristics. In jellium-model calculations,[16] where the configuration of the defect complex is ignored, the calculated positron lifetime is expected to show a monotonous decrease, with the addition of helium atoms. On the other hand, the present results bring out the sensitivity of annihilation characteristics to the defect geometry.

III. EXPERIMENTAL DETAILS

Pure Ni (99.999%) samples of size 1 cm×1cm×300 μm were annealed at 1270 K for 3 h in a vacuum of 5×10^{-6} mbar and furnace cooled to produce a defect-free reference state. These Ni samples were homogeneously helium implanted using 40-MeV α particles from the Variable Energy Cyclotron, Calcutta, in conjunction with an implantation chamber reported earlier.[37] The incoming α-particle beam passes through a rotating degrader wheel mounted with 30 aluminum foils of different thicknesses. This continuously degrades the beam energy from 40 to about 0.5 MeV, resulting in a homogeneous helium distribution over a depth of 240 μm from the surface of the Ni samples. This implantation procedure ensures a strong overlap of the helium profile with the positron profile at all depths, thereby providing a true sampling of helium regions by the positron. Three sets of Ni samples were independently implanted with helium to doses of 100, 250, and 400 at. ppm. The helium concentrations in the samples were estimated from the measured total charge on the target holder during the implantation. To obtain a reference annealing behavior of the defects, helium-free α-particle irradiation was carried out at 450±50 K to a fluence of $1.2\times10^{17}\alpha/cm^2$ on another set of Ni samples of thickness 200 μm. Since the range of 40-MeV α particles in Ni (240 μm) is higher than the thickness of the sample, most of the α particles pass through the sample, leaving behind only the displacement damage.

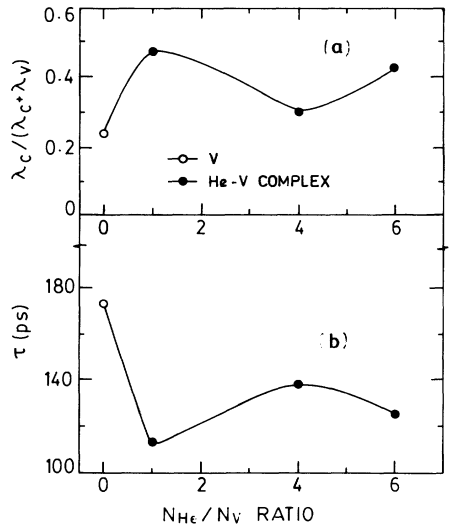

FIG. 5. Variation of (a) the normalized core-annihilation rate $\lambda_c/(\lambda_c+\lambda_v)$ and (b) positron lifetime as a function of the extent of helium decoration in a monovacancy (N_{He}/N_V ratio) in Ni. The open circles indicate the value for monovacancy, while the solid circles correspond to helium-decorated monovacancy complexes.

Post-irradiation positron-lifetime and Doppler-broadened line-shape measurements were carried out on the above Ni samples as a function of isochronal annealing temperature from 300 to 1200 K. These measurements were made at room temperature after each isochronal annealing treatment in a vacuum furnace for 30 min. Doppler-broadened line-shape measurements were carried out using a spectrometer having an energy resolution [full width at half maximum (FWHM)] of 1.1 keV for the 514-keV γ ray of ^{85}Sr. From the measured spectra at each annealing temperature, the peak line-shape parameter I_v was evaluated.[14] From the line-shape parameter I_v^f corresponding to the defect-free Ni sample and from the above I_v corresponding to the irradiated samples, a reduced line-shape parameter

$$\Delta I_v/I_v^f=(I_v-I_v^f)/I_v^f \quad (1)$$

was deduced for monitoring the defect-recovery stages. Positron-lifetime measurements were carried out using a high-resolution lifetime spectrometer[36] having a time resolution (FWHM) of 200 ps. Lifetime spectra were analyzed in terms of two components using the programs RESOLUTION and POSITRONFIT.[38] Defect recovery was also monitored using a mean lifetime τ given by

$$\bar{\tau}=I_1\tau_1+I_2\tau_2\ , \tag{2}$$

where τ_1 and τ_2 are the resolved lifetime components and I_1 and I_2 are the corresponding intensities.

IV. STUDY OF THE α-PARTICLE IRRADIATED Ni (100 at. ppm He)

The variation of the reduced line-shape parameter $\Delta I_v/I_v^f$ and the mean lifetime $\bar{\tau}$ as a function of annealing temperature is shown in Fig. 6 for helium-free α-particle-irradiated Ni. Continuous defect recovery is seen for this sample in accordance with the expected annealing behavior of irradiation-induced loops and small vacancy clusters.[39] Figure 7 shows the variation of the line-shape parameter for α-particle-irradiated Ni containing 100 at. ppm He. A comparison of the annealing curves in Figs. 6 and 7 shows the following features: (a) For both samples the line-shape parameter exhibits a sharp decrease above 500 K. (b) In α-particle-irradiated Ni (100 at. ppm He), a broad shoulder is seen between 700 and 900 K, which is absent in helium-free sample. (c) The line-shape parameter does not attain a preirradiation value even at 1170 K for Ni (100 at. ppm He), unlike that of helium-free Ni.

To understand the processes due to helium in more detail, positron-lifetime measurements were made on a Ni sample containing 100 at. ppm He. The variation of the resolved positron-lifetime parameters τ_1, τ_2, and I_2, as a function of annealing temperature, is shown in Fig. 8. In the as-irradiated state, a shorter lifetime τ_1 of 140 ps with 70% intensity and a longer lifetime τ_2 of 240 ps with 30% intensity are resolved. The computed binding-energy trends shown in Sec. II B indicate that small helium-vacancy complexes can trap positrons effectively. From the computed values of lifetimes (Table II), a lifetime of 140 ps can be assigned to a four-helium–vacancy complex (He_4V). In spite of the good agreement between the experimental τ_1 value and the computed value for the

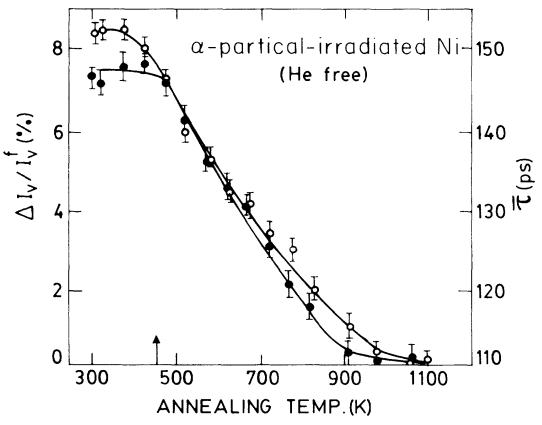

FIG. 6. Variation of the reduced line-shape parameter $\Delta I_v/I_v^f$ (solid circles) and the mean lifetime $\bar{\tau}$ (open circles) as a function of annealing temperature for helium-free α-particle-irradiated Ni (fluence $1.2\times10^{17}\alpha/\text{cm}^2$). Irradiation temperature is indicated by the arrow on the axis.

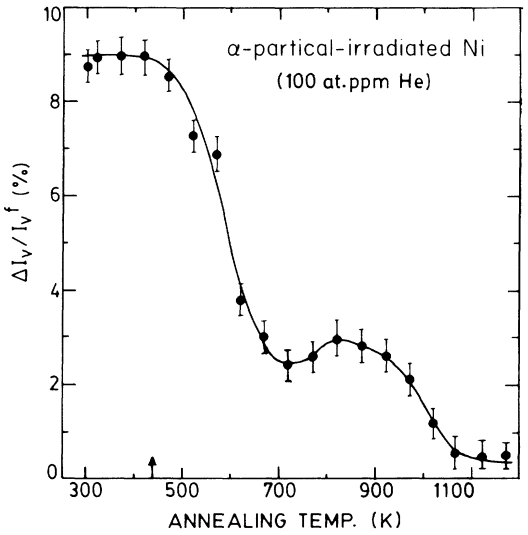

FIG. 7. Variation of the reduced line-shape parameter $\Delta I_v/I_v^f$ as a function of annealing temperature for α-particle-irradiated Ni (100 at. ppm He). Irradiation temperature is indicated by the arrow on the axis.

He_4V complex, a small contribution to the observed value of τ_1 from positron trapping at irradiation-induced dislocation loops cannot be ruled out. Accordingly, the observed τ_1 of 140 ps of dominant intensity is understood as due to the combined effect of positron trapping in small

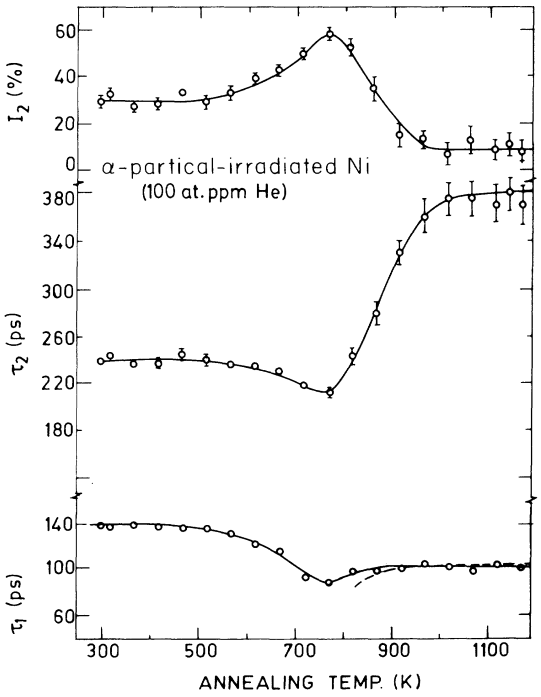

FIG. 8. Variation of the resolved positron-lifetime parameters τ_1 and τ_2 and intensity I_2 as a function of annealing temperature for α-particle-irradiated Ni (100 at. ppm He). The dashed line indicates τ_1 evaluated using the two-state trapping model.

helium-vacancy complexes and dislocation loops. The longer lifetime τ_2 of 240 ps with 30% intensity is understood as due to vacancy clusters. From the variation of the computed positron lifetime as a function of the size of the vacancy cluster, shown in Fig. 3(b), such a lifetime would correspond to a cluster of about five vacancies.

As the annealing temperature is increased, the lifetime parameters τ_1, τ_2, and I_2 remain constant up to 500 K, indicating the initial stability of irradiation-induced defect structures. Between 500 and 750 K, τ_1 decreases sharply toward a bulk-state value, τ_2 decreases, exhibiting a minimum, and the intensity I_2 increases toward a maximum. The temperature of occurrence of these stages seen in τ_1, τ_2, and I_2 matches with the onset of a shoulder seen earlier in the annealing curve of the I_v parameter (Fig. 7). The decrease of τ_1 from a value of 140 ps toward the bulk-state value indicates the dissociation of unstable helium-vacancy complexes, which is in agreement with the earlier results of thermal helium-desorption-spectroscopy studies. These THDS results[9] on helium-implanted Ni indicate a dissociation temperature of 700 K for He_nV complexes with $n=2-4$. In the same annealing interval, τ_2 decreases from an initial value of 240 to 210 ps. As seen from the computed lifetime trends in Fig. 3, positron lifetime decreases upon helium decoration of vacancy clusters. Accordingly, the observed reduction in τ_2 around 750 K may be understood as due to helium decoration of vacancy clusters. The helium supply from the dissociating He_nV complexes together with the supply of vacancies from the annealing of loops (as evident from the reduction of τ_1) lead to the nucleation of microbubbles with a critical helium-to-vacancy ratio. The increase in I_2 seen around 750 K is explained as due to enhanced positron trapping in the nucleated microbubbles. Thus the observed characteristic variation of τ_1, τ_2, and I_2 between 500 and 750 K in Fig. 8 signifies the bubble nucleation stage.

Above 750 K helium bubbles are the dominant positron traps as seen from the bulk-state behavior of τ_1, which is in accordance with the two-state trapping model. Between 750 and 1000 K, τ_2 increases sharply, with a concomitant decrease of I_2. The increase in τ_2 indicates that the bubbles relax in size, while the decrease in I_2 signifies the reduction in bubble concentration. These features are in accordance with post-nucleation bubble growth. Beyond 1000 K, τ_2 reaches a saturation value of 380 ps, while I_2 levels off to a value of about 10%. The constancy of τ_2 indicates that the helium-atom density has reached an optical value during growth. The observed features in Ni (100 at. ppm He), corresponding to the nucleation and growth of bubbles, are qualitatively similar to those reported earlier for helium-implanted copper.[22,23]

V. ANALYSIS OF BUBBLE GROWTH

Recent studies in aluminum[20] and copper[23] have shown that from an analysis of the measured positron lifetime parameters, one can determine the bubble size, concentration, and helium-atom density (pressure) in bubbles. A brief outline of the essential steps involved in the analysis scheme is given below.

A. Analysis scheme

From *ab initio* calculations of positron lifetimes in the small-cluster regime (radii typically <5 Å) reported in Sec. II, the lifetime has been shown to be sensitive to the size as well as the helium-to-vacancy ratio of the cluster. For larger bubbles observed during growth, the recent theoretical results[17,18] based on the positron surface-state model, have shown that the lifetime corresponding to bubbles is controlled by the helium-atom density alone. Accordingly, from the experimental lifetime value τ_2 corresponding to the bubbles, the helium-atom density n_{He} in the bubbles is obtained using the relation[18]

$$\tau_2(\text{ps})=500-23.5[n_{He}(10^{22}\ \text{cm}^{-3})] \ . \tag{3}$$

The above relation does not depend on the specific nature of the host metal. It thereby forms the general basis for using positron-lifetime spectroscopy in determining gas densities and pressures in bubbles.[40] Using the two-state trapping model,[14] the total trapping rate due to the bubbles, K_B, can be obtained from the measured lifetime parameters as

$$K_B=I_2(\lambda_1-\lambda_2) \ , \tag{4}$$

where λ_1 (τ_1^{-1}) and λ_2 (τ_2^{-1}) are the experimental annihilation rates and I_2 is the intensity. The total trapping rate K_B and concentration of the bubbles, C_B, are related by

$$C_B=K_B/\mu_B \ , \tag{5}$$

where μ_B is the specific trapping rate for the bubbles. Although μ_B depends on both bubble size and helium-atom density, for a given temperature, its variation with helium-atom density is expected to be weak for sufficiently large bubbles.[41] Accordingly, only the size dependence of μ_B is taken into account by using the semiempirical relation[20,41] for bubbles with $r_B \geq 5$ Å as

$$\mu_B=(1/Ar_B+1/Br_B^2)^{-1} \ , \tag{6}$$

where the constants are given by $A=9.07\times10^{15}$ Å^{-1}s^{-1} and $B=3.3\times10^{14}$ Å^{-2}s^{-1}. The bubble radius r_B can be expressed in terms of the helium-inventory equation given by

$$N_{He}=\tfrac{4}{3}\pi r_B^3 C_B n_{He} \ , \tag{7}$$

where N_{He} is the total input helium concentration. Substituting Eqs. (4)–(6) in (7) and recasting it results in a quadratic equation in r_B as

$$Br_B^2+Ar_B-3ABN_{He}/4\pi I_2(\lambda_1-\lambda_2)n_{He}=0 \ . \tag{8}$$

With n_{He} known from Eq. (3), the above equation can be solved for the average bubble radius. Knowing the value of R_B, the concentration of bubbles, C_B, can be obtained from Eq. (7). The underlying assumption in the above scheme is that all of the input helium is contained in spherical bubbles. Considering the fact that bulk samples

TABLE III. Bubble parameters for α-particle-irradiated Ni (100 at. ppm He) derived from the analysis of experimental lifetime parameters in the growth stage. T is the annealing temperature, n_{He} is the helium-atom density, r_B is the bubble radius, and C_B is the bubble concentration.

T (K)	n_{He} (nm^{-3})	r_B (nm)	C_B (10^{20} m^{-3})
820	109±10	1.5±0.3	60±10
870	91±9	2.0±0.4	29±6
920	72±7	4.3±0.8	3.7±1.2
970	59±6	5.0±1.0	2.9±1.0
1020	53±5	6.6±1.3	1.4±0.6
1070	53±5	5.6±1.1	2.4±0.9
1120	55±5	6.1±1.2	1.7±0.6
1170	55±5	6.1±1.2	1.7±0.6

of thickness ~ 100 μm are used for PAS studies, the helium loss from the bubble to the sample surface is expected to be negligible. Hence the above assumption is reasonably sound, although a slight overestimate for r_B, brought about by the assumption of zero helium loss, cannot be ruled out. The above discussed scheme enables the determination of helium-atom density, bubble radius, and bubble concentration using the PAS data.

B. Bubble parameters for Ni (100 at. ppm He)

The bubble parameters for Ni (100 at. ppm He) have been deduced for different annealing temperatures from 820 K onward, from the analysis of PAS data as per the above scheme, and are shown in Table III. The deduced bubble radius r_B and bubble concentration C_B as a function of annealing temperature are shown in Figs. 9 and 10, respectively. As seen from the figures, the average bubble radius r_B increases, while the concentration of bubbles, C_B, decreases as the annealing temperature is increased. These provide quantitative confirmation of the bubble growth.

A recent compilation[12] of data on bubble growth in Ni and the theoretical interpretation[42] have led to the conclusion that helium bubbles in the bulk retain a considerable overpressure, even up to an annealing temperature of 1200 K. The growth of these bubbles, involving a low activation energy of 0.23 eV, has been identified to be due to bubble-migration and -coalescence processes. On the other hand, there is enhanced coarsening of bubbles near the surface of Ni. The activation energy for the growth of surface bubbles has been found to be higher (1.1 eV) and has been identified with the mechanism of Ostwald ripening.[12] The existence of overpressurizing bubbles in the bulk of Ni samples has been recently confirmed by SANS results.[13] In the present PAS study, we have examined the effect of internal pressure on bubble growth to provide additional evidence on the existence of overpressurized bubbles. This is discussed below.

Figure 11(a) shows a plot of the helium-atom density n_{He} versus the bubble radius r_B, as deduced from the experimental PAS data using the analysis scheme discussed earlier. The dashed curve shown for comparison represents the densities corresponding to bubbles in thermodynamic equilibrium. This is obtained from the Trinkaus equation of state[43] and using a value of 1.8 $N m^{-1}$ for the surface free energy γ of nickel.[5] The following features can be noted from Fig. 11(a): (i) There is a clear deviation, outside the uncertainty of the deduced parameters, from the behavior expected for equilibrium bubbles. (ii) n_{He} tends to remain constant, independent of r_B for radii >5 nm. This implies that the helium density has reached an optimal value and does not relax further during growth. Figure 11(b) shows the plot of the corresponding pressure P in bubbles as a function of r_B, where P is obtained from the experimental n_{He} [Fig. 11(a)], using the Trinkaus equation of state.[43] The equilibrium pressure curve ($p = 2\gamma / r_B$) is also shown as a dashed line

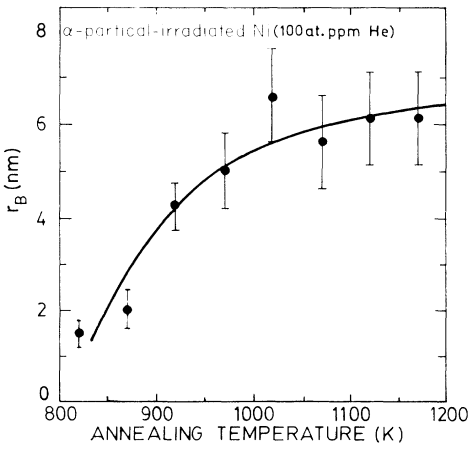

FIG. 9. Bubble radius r_B, deduced from the analysis of positron-lifetime parameters, as a function of annealing temperature for α-particle-irradiated Ni (100 at. ppm He).

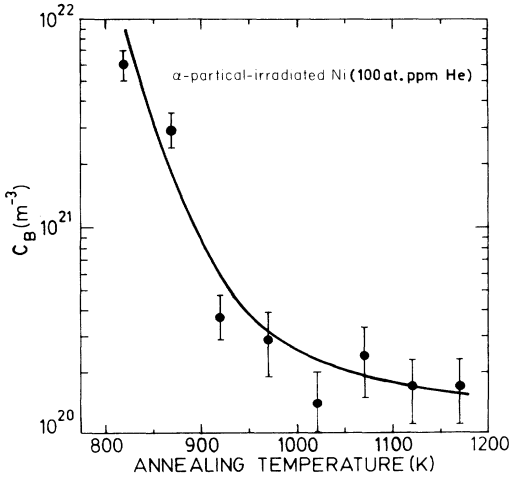

FIG. 10. Bubble concentration C_B, deduced from the analysis of positron-lifetime parameters, as a function of annealing temperature for α-particle-irradiated Ni (100 at. ppm He).

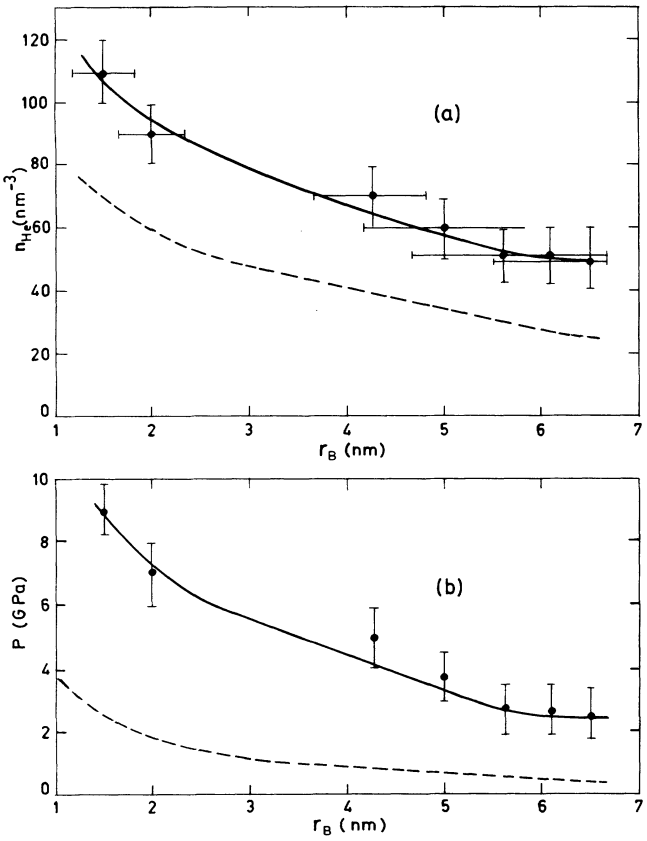

FIG. 11. (a) Plot of helium-atom density in the bubble, n_{He}, vs bubble radius r_B in Ni (100 at. ppm He). The dashed curve corresponds to equilibrium bubbles. (b) Plot of helium pressure P vs r_B. The dashed curve corresponds to equilibrium bubbles obeying the relation $P=2\gamma/r_B$.

for comparison in Fig. 11(b). It is clear from Fig. 11(b) that bubbles are overpressurized ($\Delta P \approx 3$ GPa), which might be the case if the vacancy supply is too small to relax the bubbles to equilibrium sizes. Under conditions of vacancy deficit, strong pressure-relaxation mechanisms of growth are perhaps not operating. Moreover, from the present study, an Arrhenius plot of $\ln r_B$ vs $1/T$ yields a slope of ~ 0.36 eV, which is close to the value for the activation energy for bubble growth in bulk Ni, as reported from a recent study.[12] This leads to the conclusion that a weakly activated process such as bubble migration and coalescence is operative in the present case, where the bubble can be expected to maintain their overpressure during growth. This is in agreement with recent theoretical[42] and experimental SANS (Ref. 13) results.

VI. LIFETIME STUDY ON α-PARTICLE-IRRADIATED Ni (400 at. ppm He)

Positron-lifetime measurements have also been made on a higher-dose Ni sample containing 400 at. ppm He. These spectra were analyzed for two components as well as for three components. However, the three-component analysis, constrained and unconstrained, did not yield satisfactory fits. The variation of resolved lifetime parameters as a function of annealing temperature obtained using two-component analysis is shown in Fig. 12. The irradiation temperature in the present case is 500 K, which is similar to that of Ni (100 at. ppm He) sample. In as-irradiated state, two lifetimes $\tau_1=200$ ps with 85% intensity and $\tau_2=465$ ps with I_2 of 15% are resolved. These lifetime values are higher than those of Ni (100 at. ppm He). This difference may be attributed to the formation of larger defect clusters arising from the higher concentration of point defects produced in the higher-dose Ni sample. Based on the comparison of the experimental lifetimes with the computed values shown in Fig. 3, the larger lifetime τ_2 is attributed to voids, while the shorter lifetime τ_1 is explained as due to He-V clusters. The variation of τ_1, τ_2, and I_2 as a function of annealing temperature in Fig. 12 indicates the nucleation and growth of bubbles. The observed value of the lifetime τ_2 corresponding to the nucleation temperature as well as the near-saturation value at higher annealing temperature in Fig. 12 are significantly larger than those for the lower-dose Ni sample (100 at. ppm He), thereby indicating the effect of dose on bubble characteristics.

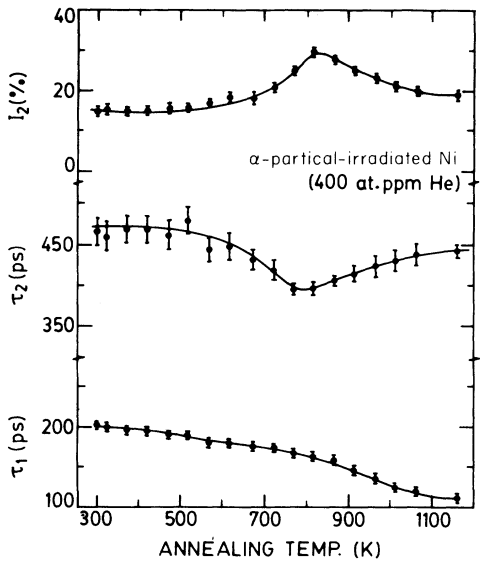

FIG. 12. Variation of the resolved lifetime parameters τ_1 and τ_2 and intensity I_2 as a function of annealing temperature for α-particle-irradiated Ni (400 at. ppm He).

VII. HELIUM-DOSE DEPENDENCE OF BUBBLE PARAMETERS

Information concerning the bubble-growth processes can also be obtained from the dependence of bubble radius and bubble concentration on input helium concentration.[44] For the bubble-migration and -coalescence model, the mean bubble radius is expected to increase as a function of input helium concentration. For the case of the Ostwald ripening model, the mean bubble radius is independent of input helium concentration. Figure 13 shows the plot of the deduced bubble radius r_B and bubble concentration C_B as a function of implanted helium

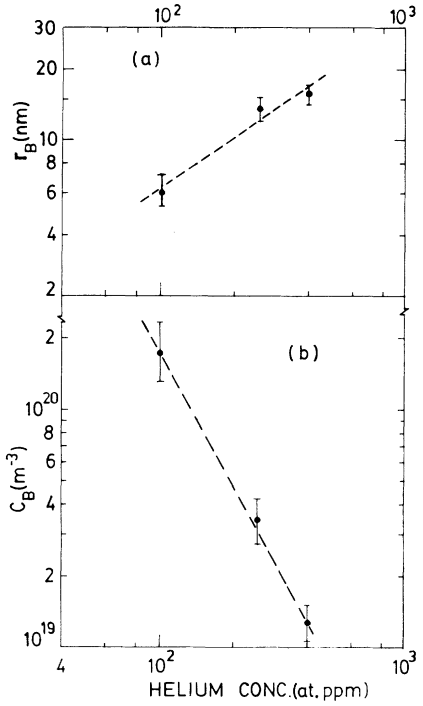

FIG. 13. Plot of (a) bubble radius r_B and (b) bubble concentration C_V vs implanted helium concentration in Ni.

concentration. Here the bubble parameters, corresponding to the intermediate helium concentration of 250 at. ppm, have been deduced from the analysis of our earlier reported data.[37] while those corresponding to doses of 100 and 400 at. ppm are from the present PAS data discussed in earlier sections. The values of r_B and C_B shown in Fig. 13 correspond to the annealing temperature of 1170 K. As seen from Fig. 13, the average bubble radius r_B increases monotonically with implanted helium concentration. This behavior would support the bubble-migration and -coalescence mechanism. The bubble concentration C_B decreases monotonically with helium concentration for the same annealing conditions. A similar dose dependence of bubble parameters has been observed in stainless steel.[45] The present conclusions on the bubble-growth mechanism, as deduced from the dose-dependence study, are consistent with the results discussed earlier in Sec. V.

VIII. SUMMARY AND CONCLUSIONS

Detailed positron-annihilation experiments, in conjunction with *ab initio* theoretical computations in helium-decorated vacancy clusters, have led to a detailed understanding of helium behavior in nickel. The theoretical results of annihilation characteristics show the dependence of lifetime on (i) the size of helium-vacancy clusters and (ii) the helium-to-vacancy ratio as well as on the configuration of multiple-helium-decorated vacancy complexes. Based on the comparison of the computed positron lifetimes with the experimental lifetimes, the observed bubble nucleation is understood as due to the supply of helium from the dissociation of unstable helium-vacancy complexes and consequent formation of microbubbles aided by vacancies from the annealing dislocation loops. From the analysis of the PAS data in the post-nucleation growth stage, the average bubble radius, bubble concentration, and helium-atom density in the bubbles have been extracted as a function of annealing temperature. An analysis of bubble growth in Ni (100 at. ppm He) indicates the existence of overpressure in bubbles, in excess of what is expected for equilibrium bubbles. The nucleation and growth behavior in higher-dose Ni (400 at. ppm He) has been studied and compared with those of Ni with 100 at. ppm He. The deduced dependence of bubble parameters on helium dose is consistent with the migration and coalescence process of bubble growth.

As a future outlook, with the emergence of slow-positron beams[46] having the capability for depth profiling of defects,[47,48] positron-annihilation spectroscopy may be expected to play an even more significant role in the study of helium in metals.

ACKNOWLEDGMENTS

The authors thank the staff of VEC, Calcutta, for their help and cooperation during α-particle-irradiation experiments. They are thankful to Dr. C. S. Sundar for a critical reading of the manuscript and D. Vasumathi, R. Rajaraman, J. Jayapandian, and P. Gopalan for their assistance. Useful discussions with Professor H. Trinkaus and Professor H. Ullmaier are gratefully acknowledged.

[1]Proceedings of the International Symposium on Fundamental Aspects of Helium in Metals, edited by H. Ullmaier, Radiat. Eff. **78**, 1 (1983).

[2]*Proceedings of NATO Advanced Workshop on Fundamental Aspects of Inert Gases in Solids,* NATO ASI Series, edited by S. E. Donnelly and J-H. Evans (Plenum, New York, 1991), p. 209.

[3]H. Ullmaier, Nucl. Fusion **24**, 1039 (1984).

[4]G. J. Thomas, Radiat. Eff. **78**, 37 (1983).

[5]S. E. Donnelly, Radiat. Eff. **90**, 1 (1985).

[6]W. Jager, P. Ehrart, and W. Schilling, Mater. Sci. Forum **15-18**, 881 (1987).

[7]V. Philipps, K. Sonnenberg, and J. M. Williams, J. Nucl. Mater. **107**, 271 (1982).

[8]P. Jung and K. Schroeder, J. Nucl. Mater. **155-157**, 1137 (1988).

[9]A. Van Veen, Mater. Sci. Forum **15-18**, 3 (1987).

[10]W. D. Wilson, C. L. Bisson, and M. I. Baskes, Phys. Rev. B **24**, 5616 (1981).

[11]J. B. Adams and W. G. Wolfer, J. Nucl. Mater. **106**, 235 (1989).

[12]V. N. Chernikov, H. Trinkaus, P. Jung, and H. Ullmaier, J.

Nucl. Mater. **170**, 31 (1990).
[13]Qiang-Li, W. Kesternich, H. Schroeder, D. Schawan, and H. Ullmaier, Acta Metall. Mater. **38**, 2383 (1990); H. Ullmaier (private communication).
[14]See, for example, *Positron Solid State Physics,* edited by W. Brandt and A. Dupasquier (North-Holland, Amsterdam, 1983).
[15]R. W. Siegel, Annu. Rev. Mater. Sci. **10**, 393 (1980).
[16]P. Jena and B. K. Rao, Phys. Rev. B **31**, 5634 (1985).
[17]K. O. Jensen and R. M. Nieminen, Phys. Rev. B **35**, 2087 (1987).
[18]K. O. Jensen and R. M. Nieminen, Phys. Rev. B **36**, 8219 (1987).
[19]H. E. Hansen, H. Rajainmaki, R. Talja, M. D. Bentzon, R. M. Nieminen, and K. Petersen, J. Phys. F **15**, 1 (1985).
[20]K. O. Jensen, M. Eldrup, B. N. Singh, S. Linderoth, and M. D. Bentzon, J. Phys. F **18**, 1069 (1988).
[21]H. Rajainmaki, R. M. Nieminen, S. Linderoth, H. E. Hansen, and M. D. Bentzon, Phys. Rev. B **38**, 1087 (1988).
[22]B. Viswanathan, G. Amarendra, and K. P. Gopinathan, Radiat. Eff. **107**, 121 (1989).
[23]G. Amarendra, B. Viswanathan, and K. P. Gopinathan, Radiat. Eff. Def. Solids (to be published).
[24]B. Viswanathan, W. Triftshauer, and G. Kogel, Radiat. Eff. **78**, 231 (1983).
[25]S. V. Naidu, A. Sen Gupta, G. Mukhopadhyay, R. K. Bhandari, and P. Sen, Radiat. Eff. **83**, 129 (1984).
[26]G. Kogel, Q. M. Fan, P. Sperr, W. Triftshauser, and B. Viswanathan, J. Nucl. Mater. **127**, 125 (1985).
[27]G. Amarendra and B. Viswanathan, in *Positron Annihilation,* edited by L. Dorikens-Vanpraet, M. Dorikens, and D. Segers (World Scientific, Singapore, 1989), p. 494.
[28]M. J. Puska and R. M. Nieminen, J. Phys. F **13**, 333 (1983).
[29]A. Bharathi and B. Chakraborty, J. Phys. F **18**, 363 (1988).
[30]J. Arponen and E. Pajanne, Ann. Phys. (N.Y.) **121**, 343 (1979).
[31]F. Herman and S. Skillman, *Atomic Structure Calculations* (Prentice-Hall, Engelwood Cliffs, NJ, 1963).
[32]W. Brandt and J. Reinheimer, Phys. Lett. **35A**, 109 (1971).
[33]H. E. Hansen, R. M. Nieminen, and M. J. Puska, J. Phys. F **14**, 1299 (1984).
[34]J. R. Beeler, Jr., *Radiation Effects and Computer Experiments* (North-Holland, Amsterdam, 1983).
[35]M. I. Baskes and C. F. Melius, Phys. Rev. B **20**, 3197 (1979).
[36]G. Amarendra, Ph.D. thesis, University of Madras, Madras, 1990.
[37]G. Amarendra, B. Viswanathan, and K. P. Gopinathan, Cryst. Res. Technol. **22**, 1563 (1987).
[38]P. Kirkegard, M. Eldrup, O. E. Mogensen, and N. J. Pedersen, Comput. Phys. Commun. **23**, 307 (1981).
[39]C. S. Sundar, A. Bharathi, and K. P. Gopinathan, Philos. Mag. A **50**, 635 (1984).
[40]K. O. Jensen (private communication).
[41]K. O. Jensen, M. Eldrup, B. N. Singh, A. Horswell, M. Victoria, and W. F. Somer, Mater. Sci. Forum **15-18**, 913 (1987).
[42]H. Trinkaus, Scr. Metall. **23**, 1773 (1989).
[43]H. Trinkaus, Radiat. Eff. **78**, 189 (1983).
[44]J. Routhaut, H. Schroeder, and H. Ullmaier, Philos. Mag. A **47**, 781 (1983).
[45]P. Batfalsky and H. Schroeder, J. Nucl. Mater. **122-123**, 1475 (1984).
[46]P. J. Schultz and K. G. Lynn, Rev. Mod. Phys. **60**, 701 (1988).
[47]W. Triftshauser and G. Kogel, Phys. Rev. Lett. **48**, 1741 (1982).
[48]K. G. Lynn, D. M. Chen, B. Nielsen, R. Pareja, and S. Mayers, Phys. Rev. B **34**, 1449 (1986).